

Searching for Cosmic Strings in CMB Anisotropy Maps using Wavelets and Curvelets

Lukas Hergt,^{1,*} Adam Amara,^{1,†} Robert Brandenberger,^{2,‡} Tomasz Kacprzak,^{1,§} and Alexandre Réfrégier^{1,¶}

¹*ETH Zurich, Department of Physics, Wolfgang-Pauli-Strasse 27, 8093 Zurich, Switzerland*

²*Physics Department, McGill University, Montreal, QC, H3A 2T8, Canada, and
Institute for Theoretical Studies, ETH Zürich, CH-8092 Zürich, Switzerland*

(Dated: March 2, 2022)

We use wavelet and curvelet transforms to extract signals of cosmic strings from cosmic microwave background (CMB) temperature anisotropy maps, and to study the limits on the cosmic string tension which various ongoing CMB temperature anisotropy experiments will be able to achieve. We construct sky maps with size and angular resolution corresponding to various experiments. These maps contain the signals of a scaling solution of long string segments with a given string tension $G\mu$, the contribution of the dominant Gaussian primordial cosmological fluctuations, and pixel by pixel white noise with an amplitude corresponding to the instrumental noise of the various experiments. In the case that we include white noise, we find that the curvelets are more powerful than wavelets. For maps with Planck specification, we obtain bounds on the string tension comparable to what was obtained by the Planck collaboration [1]. Experiments with better angular resolution such as the South Pole Telescope third generation (SPT-3G) survey will be able to yield stronger limits. For maps with a specification of SPT-3G we find that string signals will be visible down to a string tension of $G\mu = 1.4 \times 10^{-7}$.

I. INTRODUCTION

Cosmic strings are linear topological defects which exist as solutions in a large class of particle physics models beyond the Standard Model. Cosmic strings have common features with line defects in crystals and with vortex lines in superconductors and superfluids. Cosmic strings are lines of trapped energy density, and as such they have gravitational effects on space-time which lead to cosmological signals (for reviews on cosmic strings see e.g. [2–4]).

If nature is described by a particle physics model which has cosmic string solutions, then a network of strings inevitably forms during a phase transition in the early universe and persists to the present time. This is a causality argument which is originally due to Kibble [5]. Hence, the gravitational effects of the strings are unavoidable. The gravitational effects of strings are characterized by a single number, namely the tension μ (or $G\mu$ in terms of a dimensionless variable, where G is Newton’s gravitational constant). Since cosmic strings are relativistic, the tension equals the energy per unit length. The tension is given by the energy scale η of the particle physics model

$$\mu \simeq \eta^2. \quad (1)$$

Hence, the gravitational effects of cosmic strings increase as the energy scale of the particle physics model increases. Searching for cosmological signatures of strings is hence a way to test particle physics models “from top down”

(the effects are larger the higher the value of η is) and is complementary to accelerator investigations which probe particle physics models “from bottom up” (the effects are larger the lower η is - see e.g. [6] for an elaboration on this point).

The network of cosmic strings consists of infinite strings with a mean curvature radius and separation of ξ , and a distribution of string loops with radii $R < t$, where t is the time. Causality tells us that

$$\xi(t) \leq t \quad (2)$$

at all times after the phase transition during which the string network forms [5], including the present time. If the strings form during a typical symmetry breaking phase transition, then, at the time of formation, the network of cosmic strings is very dense, i.e. $\xi(t) \ll t$. The late time behaviour of $\xi(t)$ can be obtained from a Boltzmann equation which describes how the infinite string network loses energy by splitting off string loops. The result of solving this Boltzmann equation is [2–4]

$$\xi(t) \sim t \quad (3)$$

at all late times. Thus, the network of strings becomes *scale-invariant* in the sense that the statistical properties do not depend on time if all lengths are scaled to the horizon t . The network thus consists of a few infinite strings crossing each horizon volume, the strings having typical curvature radius proportional to t , and a distribution of loops. In this article we will focus on the signals of the infinite strings since they lead to signatures with particular geometrical patterns in position space maps.

The gravitational signatures of strings are due to the fact that space perpendicular to a string is conical with deficit angle [7]

$$\alpha = 8\pi G\mu. \quad (4)$$

*Electronic address: hergtl@phys.ethz.ch

†Electronic address: adam.amara@phys.ethz.ch

‡Electronic address: rhb@physics.mcgill.ca

§Electronic address: tomasz.kacprzak@phys.ethz.ch

¶Electronic address: alexandre.refregier@phys.ethz.ch

This deficit angle is visible up to a horizon distance in perpendicular direction from the string, where it rapidly decreases to zero [8].

The conical structure of space perpendicular to a long string leads to the *Kaiser-Stebbins* effect [9]: radiation passing on the two sides of a moving string experiences a lensing Doppler shift of magnitude

$$\frac{\Delta T}{T} = 8\pi G\mu v_s \gamma_s, \quad (5)$$

where v_s is the string velocity and γ_s is the associated relativistic γ factor. This effect leads to an interesting signal of strings in cosmic microwave background (CMB) temperature anisotropy maps: strings will lead to a network of line discontinuities which are caused by the lensing of the CMB photons by strings which the photons pass while travelling from the time t_{rec} of recombination until today $t = t_0$. The characteristic length scale of these lines is given by the comoving horizon at the time t when the photons pass by the string (e.g. about one degree in the sky for strings close to t_{rec}), and the depth of the signal is also comparable to this scale.

The density perturbations due to strings cannot be the dominant source of fluctuations in the Universe (as was initially hoped in the 1980s - see e.g. [10–12]). The reason is that fluctuations from strings are incoherent and active and do not lead to acoustic oscillations in the CMB angular power spectrum [13]. In fact, the observation of these oscillations provides a tight upper bound on the cosmic string tension [1, 14, 15]

$$G\mu \lesssim 10^{-7} \quad (6)$$

(the precise coefficient depends on the specific cosmic string evolution simulation used). Cosmic strings are hence only a supplementary source of fluctuations. However, they lead to characteristic patterns in a number of observational windows (see e.g. [16]).

Most of the signatures of long cosmic strings are due to the fact that moving strings present at time t generate regions of twice the background density in their wake [17]. These *string wakes* are nonlinear fluctuations of comoving dimension

$$z(t)[t, v_s \gamma_s t, 4\pi G\mu v_s \gamma_s t], \quad (7)$$

where $z(t)$ is the redshift at time t . Wakes lead to planar overdensities of galaxies and hence to direct B-mode CMB polarization [18] - rectangles in the sky with a uniform polarization direction and a linearly growing amplitude. Wakes at high redshift also lead to thin slices in 21cm redshift surveys where there is extra absorption [19]. The signatures of wakes are more prominent at high redshifts than at low redshifts since the wakes get disrupted by the dominant Gaussian perturbations at late times (see [20] for a study of wake disruption).

The overall angular power spectra or Fourier spectra of cosmic string signals is scale-invariant and hence hard to distinguish from the effects of the dominant Gaussian

fluctuations (the fluctuations produced by the dominant source, e.g. the Λ CDM fluctuations). This is shown e.g. in the computation of the angular power spectrum of B-mode CMB polarization [21] which yields a result which is degenerate in shape with the B-mode polarization induced by lensing of the E-mode polarization. Hence, to be able to efficiently search for strings it is more promising to analyze position space maps.

We will here explore the power of wavelets and curvelets (see e.g. [22] for an introduction to wavelet analysis, and [23] for an introduction to curvelets) to find signatures of cosmic strings in CMB temperature maps. There have been some initial efforts at searching for strings in position space CMB temperature maps in [24] and [25], the latter using a matched filtering analysis. Later on, the power of the Canny Edge Detection algorithm [26] to detect strings was explored in [27]. The analysis of [27] showed that the Canny algorithm might allow the bounds on the cosmic string tension to be reduced by close to a factor of 10 compared to what can be obtained in Fourier space when considering $10^\circ \times 10^\circ$ degree maps of the sky at $1'$ resolution, specifications chosen to correspond to the South Pole Telescope [28] and Atacama Cosmology Telescope [29] projects ¹.

The Canny algorithm looks for edges in temperature maps where the gradient of the temperature is large and where the direction of the gradient does not change much. Such an algorithm is suitable to find the Kaiser-Stebbins edges in CMB maps produced by strings, but it turns out that the long edges get disrupted by the Gaussian noise, and that the algorithm is hence not optimal. We are here searching for an algorithm which allows the effects of the long strings to stand out even in the presence of Gaussian noise, and we here show that wavelet and curvelet analysis can provide a method.

In the following, we first describe the CMB temperature maps which we have constructed. They contain contributions of a scaling network of long cosmic string segments, *Gaussian noise*, by which we mean the Gaussian fluctuations which the standard Λ CDM model would provide, and instrumental noise. Our basic maps cover $12.8^\circ \times 12.8^\circ$ sections of the sky at $1.5'$ resolution. By combining such maps and by smoothing out the resulting maps we can construct maps relevant to the characteristics of various ongoing experiments such as Planck [30] or the South Pole Telescope (SPT) project. We then introduce the wavelet and curvelet transforms which we use, and describe their application to the temperature maps. We compare the potential of various experiments to detect cosmic string signals, and we find that the SPT-3G experiment [31] will be able to identify string signals down to a string tension of $G\mu = 1.4 \times 10^{-7}$, a value comparable to the current best limits [1, 14] which are

¹ Note, however, that instrumental noise effects were not considered in [27].

derived from fitting the angular power spectrum of the CMB. Note that in the absence of instrumental noise, signals are visible by eye down to a tension of $G\mu = 5 \times 10^{-8}$, and that the signals can be picked out by a simple histogram statistic down to a value of $G\mu = 3 \times 10^{-8}$, a significantly better performance than what can be achieved using the Canny algorithm. With instrumental noise effects included our limit from maps of SPT-3G specification is $G\mu < 1.4 \times 10^{-7}$.

Searches for the non-Gaussian signals of cosmic strings were also performed by the Planck collaboration [1] using Minkowski functionals and steerable wavelets (see also [32] for a discussion of the method). The constraints obtained from these analyses are comparable to the ones we obtain for simulations with the size, angular resolution and noise level of the Planck maps. Our work is complementary to the analysis by the Planck collaboration. The analysis of [1] is based on cosmic string temperature maps generated from the numerical string network simulations of [33]². Hence, these maps contain both the signals from long strings and from loops, and they take into account the fact that the long string segments can have small-scale structure. On the other hand, the analysis is subject to numerical uncertainties in the simulations. Our analysis is based on toy model string maps produced by long string segments without small-scale structure. The signals we find are hence due to the purely stringy nature of the maps. Our approach also allows us to vary the parameters which describe the cosmic string network. It is satisfying that our results for maps with Planck specification match with those obtained in [1].

Note that, following the usual conventions in the cosmic string literature, we are using natural units in which the speed of light c , Planck's constant and the Boltzmann constant are set to 1.

II. SIMULATIONS

For this work we have produced new CMB temperature maps which are the superposition of three maps, one due to Gaussian noise, the second due to cosmic strings, and the third due to instrumental noise. Our basic maps have an angular scale of $12.8^\circ \times 12.8^\circ$ and an angular resolution of $1.5'$, yielding maps with 512×512 pixels. Further down, these properties and the pixel by pixel white noise will be matched to various ongoing experiments.

The first map corresponds to what a vanilla Λ CDM cosmological model would predict. The angular power spectrum C_l was computed using the CAMB code [35]. Like in [27], the Fourier space temperature map was con-

structed from this according to

$$\Delta T_G(k_x, k_y) = \sqrt{\frac{C_l(k_x, k_y)}{2}} (g_1(k_x, k_y) + i g_2(k_x, k_y)), \quad (8)$$

where g_1 and g_2 are normally distributed random variables with mean zero and variance one. The position space maps are then computed by taking the inverse Fourier transform

$$\Delta T_G(x, y) = iFFT[\Delta T_G(k_x, k_y)], \quad (9)$$

where $iFFT$ stands for the inverse Fourier transform. In order to obtain angular resolution of $1.5'$ it is necessary to compute the angular power spectrum up to beyond $l = 10'000$. The top left panel of Figure 1 shows a specific realization of the “pure Gaussian” map. The total angular size is $12.8^\circ \times 12.8^\circ$, and the angular resolution is $1.5'$.

Next we construct maps which correspond to what a scaling distribution of long strings would produce. We adopt the one-scale toy model of the distribution of long strings [36] described above. Furthermore, following what was done in [27], we divide the long strings into segments, and consider the segments to persist for one Hubble time and to be uncorrelated on longer time scales. In [27], the string segments at time t were considered to be straight lines with a fixed length $c_1 t$ with some constant c_1 . This procedure has two problems: firstly it does not take into account the curvature of typical long strings (the mean curvature radius is t). Secondly, the procedure introduces unphysical ends to the string segments. Here we adopt a new procedure which overcomes these two problems. We model the string segments as sections of circles, and we connect the sections such as to avoid artificial ends. Given the sky patch we simulate, the idea of the simulation is to add up the temperature fluctuations by each string which contributes to the temperature variations in this patch.

Specifically, we independently simulate a cosmic string map for time steps between the time of recombination until today

$$t_{n+1} = \alpha t_n \quad (10)$$

with $\alpha = 2$. For each time step we compute the corresponding comoving Hubble distance corresponding to the curvature radius of the strings:

$$d_c(t_{n+1}) = \alpha^{1/3} d_c(t_n), \quad (11)$$

where here $t_0 = t_{rec}$ is the time of recombination, the beginning of the first simulation interval, and

$$d_c(t_{rec}) \simeq 1.8^\circ. \quad (12)$$

At each time step we then randomly pick a first midpoint of a circular string segment with a randomly picked angular size uniformly distributed in the interval $[0, \pi]$. At the endpoints of that string segment the next segments

² See also [34] for other cosmic string evolution simulations.

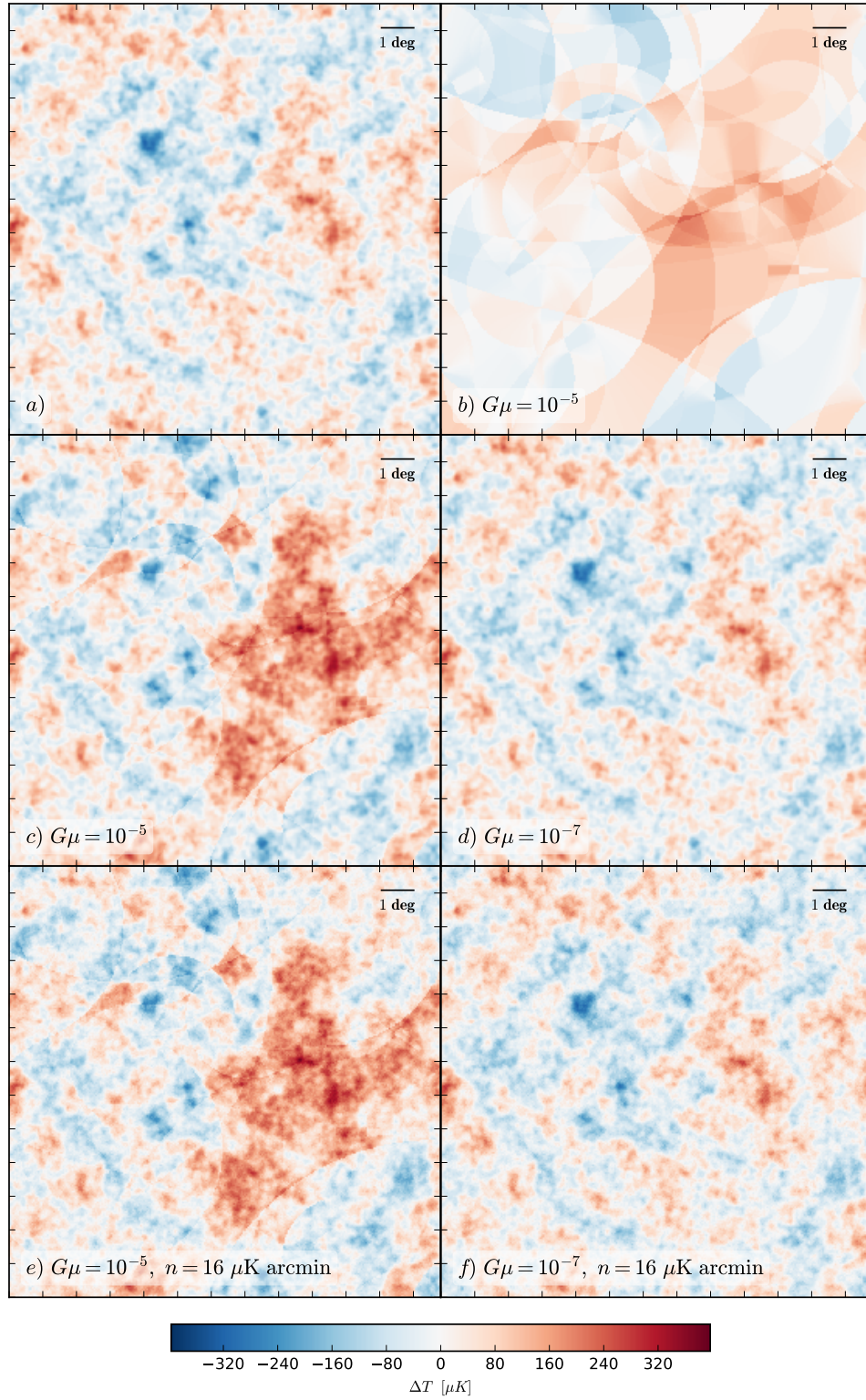


FIG. 1: Anisotropy maps of angular size $12.8^\circ \times 12.8^\circ$ and angular resolution of $1.5'$. The top left panel comes from a particular realization of the Λ CDM Gaussian CMB temperature map (no strings and no instrumental noise). The top right panel is a map from a simulation with only strings with a tension given by $G\mu = 10^{-5}$. The two medium panels are from simulations which include both Gaussian noise and string signals, with the values of $G\mu$ indicated. With the higher value of $G\mu$ the string signals are visible by eye, but not with the lower value. The bottom two panels show to which extent the string signals are degraded when instrumental noise (at the level of the SPT-SZ experiment) is included. The color indicates temperature.

are placed, continued until the string exits the map plus an additional Hubble distance. The segments connect smoothly. We then pick another midpoint and repeat the procedure until the number of strings per Hubble volume per time step is $N = 3$.

Given the string curvature, the strings will be moving towards their center, thus creating a cooler patch inside the circle segment and a hotter patch outside, according to the equation

$$\Delta T = 8\pi G\mu \frac{\tilde{v}r}{2} T, \quad (13)$$

where T is the mean CMB background temperature, $\tilde{v} = 0.15$ (taken from the simulations of [37]) is the maximal string velocity factor $v_s\gamma_s$, and r is a random variable uniformly distributed in the interval $[0,1]$ to take into account different velocities and projection effects. The width of the temperature patterns are chosen to be a fraction $f = 1/2$ of the respective Hubble radius. Since the connecting point of the string segments cannot move to the center of each circle at the same time, it must have zero velocity. Hence, we linearly interpolate \tilde{v} from one patch to the next over a fraction of 20% of the segment length.

The top right panel of Figure 1 shows the temperature map from one pure cosmic string simulation with a value of $G\mu = 10^{-5}$. The angular extent and resolution are the same as in the top left panel, as in all other panels of this figure. The map represents a superposition of the signals from strings in all Hubble time intervals. The shorter edges are due to strings which influence photons on our past light cone at early times, the longer edges come from strings at later times. The color indicates temperature, $G\mu$.

The combined maps of Gaussian and cosmic string simulations are obtained via

$$\Delta T_{total}(x, y) = \Delta T_G(x, y) + G\mu \Delta T_{CS}(x, y), \quad (14)$$

where the first term on the right hand side is what a Planck-normalized Λ CDM model predicts, and ΔT_{CS} is the contribution of cosmic strings with $G\mu = 1$. Note that as $G\mu$ varies, the total power in the anisotropy maps changes. But for the values of $G\mu$ which we are interested in ($G\mu < 10^{-7}$) the difference in normalization is unimportant.

The middle left panel of Figure 1 shows the results of a simulation with $G\mu = 10^{-5}$. In this map, the edges produced by the strings are still visible by eye. But for the value $G\mu = 10^{-7}$, the current upper bound on the string tension, the edges are no longer visible, as shown in the middle right panel. In the following section we will show that by applying wavelet or curvelet transforms to this map, the string signals can be made to stick out by eye.

Finally, we add to the joint cosmic string and Gaussian maps a third map which corresponds to instrumental noise. We model this instrumental noise as a pixel

by pixel white noise contribution with fixed noise level whose value is a free parameter and which can be chosen to match the expected levels in various experiments.

The bottom two panels of Figure 1 show the resulting maps for the cosmic string parameters $G\mu = 10^{-5}$ (left panel) and $G\mu = 10^{-7}$ (right panel) used before, with a noise level corresponding to that of the SPT-SZ experiment.

III. WAVELET AND CURVELET ANALYSIS

The wavelet transform (see e.g. [22] for an introduction) is a method to analyze maps which is orthogonal to Fourier analysis. In Fourier analysis we expand the maps into basis functions which are plane waves, and thus maximally delocalized in position space but maximally localized in momentum space. Fourier analysis is very useful in early universe cosmology to characterize fluctuations if they are generated by a quantum vacuum process like in inflation. In this case, the Fourier mode of each field satisfies a harmonic oscillator equation and is quantized independently. The Fourier spectrum hence contains the full information about the system (modulo nonlinearities introduced through the dynamical evolution). On the other hand, topological defects such as cosmic strings produce maps which have special features in position space. These features are washed out in a typical power spectrum based on Fourier modes.

The wavelet analysis is based on decomposing the map into a set of basis functions which are localized in both frequency and position space. Hence, wavelets have the potential of yielding a better way to identify cosmic string signals in cosmological maps.

Like in the case of Fourier transformation in which the basis functions we expand in are obtained via the scaling of a basic plane wave, the wavelet transform uses a basis of functions obtained by scaling some “mother” function. In this work we used the Daubechies *db12* mother function [38]. We focus on the case of a two-dimensional map. Starting with the original image, we construct a first level *scaling image*, which in the case of the simple Haar wavelet is a map with four times less pixels, the pixels representing the average of the values of the map of four neighboring pixels. In the case of the Haar wavelet, the wavelet transform then takes the differences between these four pixels, yielding three *details images* which represent the differences in the values of the map in horizontal, vertical or diagonal direction (the *horizontal details image*, *vertical details image* and *diagonal details image*, respectively). For the Daubechies *db12* wavelet which we use the geometrical interpretation of the four first level images is a bit more complicated. The full information of the original map is contained if we consider the scaling image plus the three details images. The first level decomposition is also referred to as *finest scale*. The second level transform is then obtained by repeating the previous procedure and applying it to the scaling image.

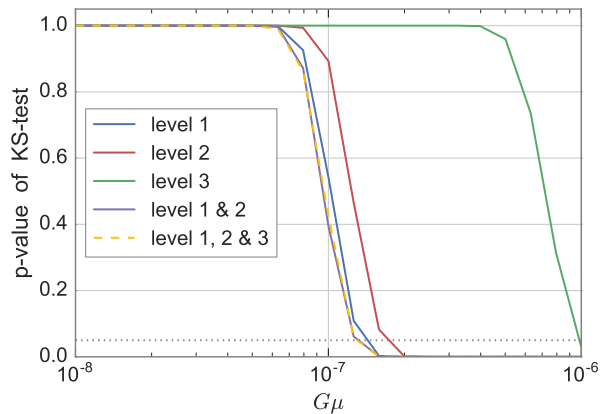


FIG. 2: Comparison of the limits on the cosmic string tension which can be obtained using curvelet analyses maps with SPT-3G specification, as a function of the level of the curvelet images used (all angles included). The horizontal axis is the string tension, the vertical axis gives the p-value from a KS test. The dotted horizontal line gives the 0.05 p-value below which a detection of the string signal is considered significant.

The computations were done using the Python package “PyWavelets” (the module named *pywt*).

We next explored the potential of a curvelet analysis to detect cosmic strings. Curvelets are defined through a partitioning of frequency space. One curvelet is obtained through rotation and translation of a mother curvelet that is the Fourier transform of a polar wedge in frequency space, defined by the support of a radial and an angular window with scale dependent window widths. Curvelets were introduced [23, 32] to track discontinuities along edges and as such appear ideal to detect signatures of cosmic strings. Hence, curvelets should be even better suited to identify cosmic string signals than wavelets.

In this work we have used Demanet’s fast discrete curvelet transform via edge wrapping for Matlab [39]. The resulting images are complex valued. For the purpose of histograms the real and the imaginary images are concatenated. The curvelet images are labeled by level and by angle. The best results are obtained by making use of the two lowest level coefficients including all angles. Figure 2 shows a comparison of how well a KS test can extract a cosmic string signal for maps with SPT-3G specification, as a function of the level of the curvelet images. The horizontal axis is the string tension, the vertical axis gives the p-value of the KS test. It is evident that Level 1 gives stronger results than higher levels. By combining Levels 1 and 2, slightly tighter limits can be obtained than by using Level 1 maps alone.

In the following section we present the results of our wavelet and curvelet analysis of CMB temperature anisotropy maps.

IV. RESULTS

We first discuss the results of our wavelet analysis. Figure 3 shows the wavelet decomposition of our maps (without instrumental noise) up to the second level in the case of combined Gaussian / string fluctuations with a value of $G\mu = 10^{-7}$. The top left quadrant shows the second level scaling and details images, the top right quadrant shows the first level horizontal details image, the bottom left the first level vertical details image, the bottom right the diagonal details image. For this value of $G\mu$, the string signals were not visible by eye in the original map, but they are clearly visible in the diagonal details image at first level. This demonstrates the promise that the wavelet method has at identifying string signals.

The panels of Figure 4 show the first level diagonal details images for the value $G\mu = 10^{-7}$ without (left panel) and with (right panel) instrumental noise. Without noise, the string signals are visible by eye, but with noise (noise levels of the SPT-SZ experiment) they are no longer visible.

Let us, for the moment, turn off instrumental noise. Then, if we further reduce the value of $G\mu$ from that used in the left panel of Figure 4, then the string signals eventually are no longer visible by eye in the first level diagonal details image. However, with statistical analyses of this details map we can probe deeper. We have only explored a very simple statistic, namely the kurtosis of the histogram of the values of the map. The histogram of a Gaussian map is Gaussian and hence its extra kurtosis is zero. The diagonal details map of a pure string map is, on the other hand, characterized by a few points with a very large value while most points have very small amplitude (the large amplitude points are along the strings). Hence, the map has a large kurtosis. The combined map will have a non-vanishing kurtosis coming from the contributions of the strings. Figure 5 shows the histogram of the diagonal details map for the case $G\mu = 10^{-7}$ (once again without instrumental noise). The non-Gaussian

	$G\mu$	k	p_k
Gaussian map		-0.011	0.561
CS map	(all)	35.702	< 0.001
combined maps	1×10^{-7}	3.217	< 0.001
	5×10^{-8}	0.327	< 0.001
	4×10^{-8}	0.137	< 0.001
	3×10^{-8}	0.037	0.048
	2×10^{-8}	-0.003	0.883
	1×10^{-8}	-0.012	0.537

TABLE I: Excess kurtosis k from the diagonal details image of the 1st level wavelet decomposition of one map and p-value p_k from the kurtosis test for different values of the string tension $G\mu$. (without white noise)

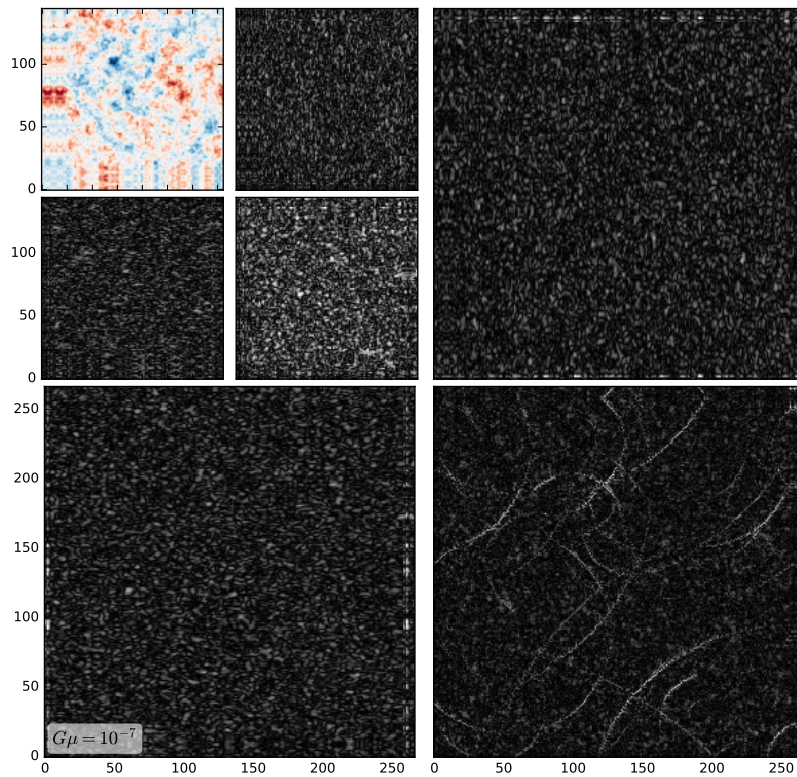


FIG. 3: Wavelet decomposition up to second level of the combined CMB anisotropy map (without instrumental noise) for a value of $G\mu = 10^{-7}$. The bottom right panel gives the diagonal details image, the image which is best for finding string signals. The other panels are described in the main text. The string signal is clearly visible by eye in the diagonal details image even though it is not visible by eye in the original map.

contribution due to strings is visible by eye for large absolute values. In Table I we give the value of the kurtosis k and the related p-value p_k under the hypothesis that the kurtosis is consistent with a Gaussian distribution for various values of $G\mu$ in the range between 10^{-8} and 10^{-7} . The bottom line is that, in the absence of instrumental noise, with a false probability of less than 5%, strings could be identified down to a value of $G\mu = 3 \times 10^{-8}$, a factor of 3 below the current limits.

However, adding pixel by pixel white noise to mimic instrumental noise degrades the results substantially. The reason is that the white noise has most power on the small scales where in position space the cosmic string signal is concentrated. The right panel of Figure 4 shows the wavelet diagonal details image for the same parameters as used in the left panel, but including white noise with the level of the SPT-SZ experiment. As is evident, the string signal is now no longer visible.

Next we turn to the results of the curvelet analysis. The panels in Figure 6 show the curvelet reconstruction of the map from finest scale coefficients. The left panel corresponds to a simulation with both Gaussian noise and cosmic strings with a tension of $G\mu = 10^{-7}$ but without instrumental white noise. The strings are visible by eye. As in the case of wavelets, the stringy features lead to a

large kurtosis of the histogram of pixel amplitudes of the map. If the string tension is lowered further, the string signals are no longer visible by eye, but they remain identifiable via the kurtosis of the histogram, namely an excess in the number of pixels with large absolute values which correspond to points lying along the strings.

In Table II we give analogously to Table I the value of the kurtosis k and the associated probability p_k that the result could be from a Gaussian distribution, for values of $G\mu$ in the interval $[10^{-8}, 10^{-7}]$ (in the absence of white noise). We see that the probability for deviations from a Gaussian distribution is significant down to a value of $G\mu = 3 \times 10^{-8}$.

Once again, adding instrumental noise degrades the power of the curvelet method. In the right panel of Figure 6 we show the CMB anisotropy map reconstructed from finest scale curvelets for the same cosmic string parameter as in the left panel, but this time including instrumental white noise with the amplitude of the SPT-SZ experiment. The string signal has been washed out.

Finally, we compared the limits on the cosmic string tension which can be obtained from various ongoing experiments, specifically three stages of the South Pole Telescope (SPT) experiment - SPT-SZ [40], SPTpol [41]

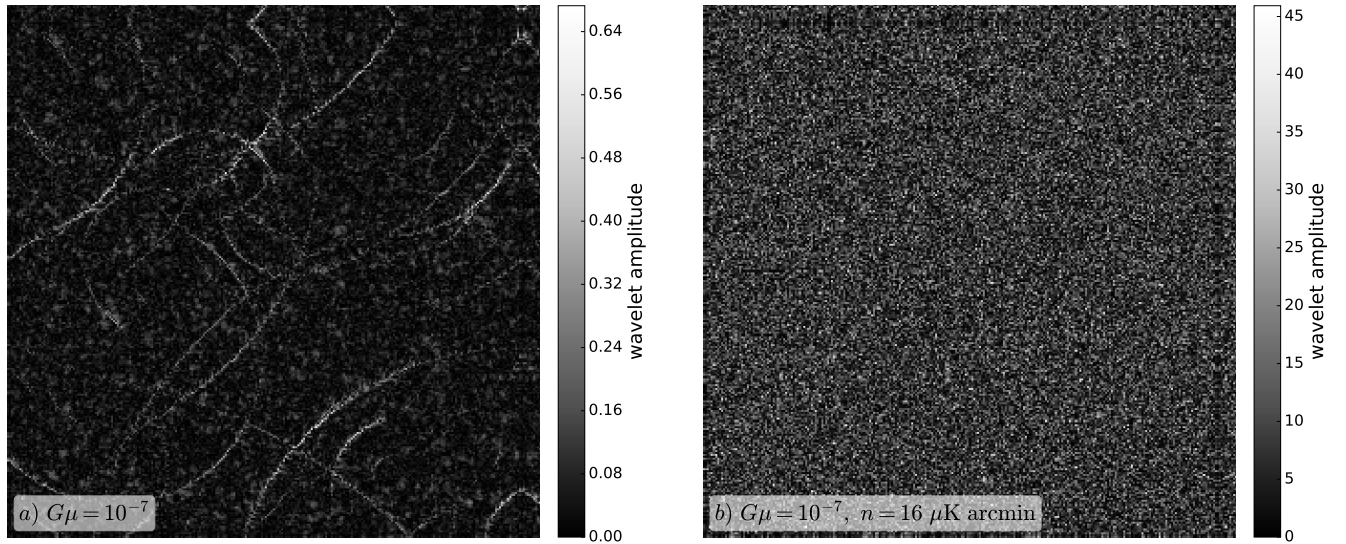


FIG. 4: Diagonal details image at first level for a CMB anisotropy map with and without instrumental noise and for the string tension given by $G\mu = 10^{-7}$. The left panel is without instrumental noise, and the string signals are visible by eye. In the right panel (which includes instrumental noise at the level of the SPT-SZ experiment) the string signal is no longer visible by eye.

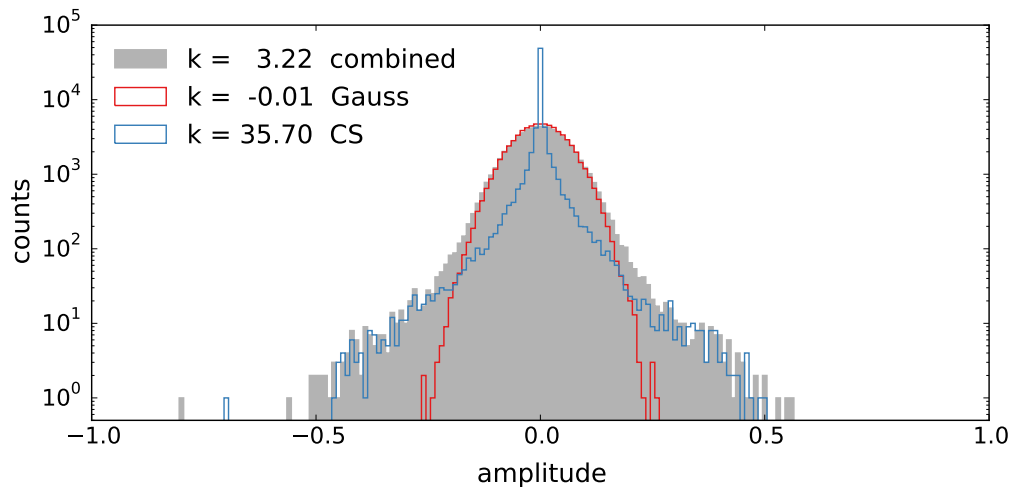


FIG. 5: Histogram of the values in the diagonal details image of the wavelet decomposition of the map with Gaussian fluctuations plus strings with $G\mu = 10^{-7}$ but without instrumental noise (Figure 4a). The kurtosis due to the large map values along the strings is visible by eye.

and SPT-3G [31] - and the Planck survey [30]³. We constructed maps with size, angular resolution and instrumental noise appropriate to these surveys (the parameters used are given in Table III). We computed the wavelet and curvelet transforms of maps with and without cosmic strings (in addition to Gaussian pri-

mordial fluctuations and white noise), and performed a Kolmogorov-Smirnov (KS) analysis for the p-value for which the string signal is visible as a function of the cosmic string tension $G\mu$. In the case of the wavelet analysis, we used the finest scale diagonal details images, for the curvelet analysis we used the first two levels and all angles. The results are given in Figure 7 and Table III.

We see that the curvelet analysis provides stronger limits than the wavelet analysis. This result is easy to understand since curvelets are better adapted to linear signals than wavelets, and thus more robust to the added

³ For Planck we have used the properties of the 143 GHz, for SPT the 150 GHz channel.

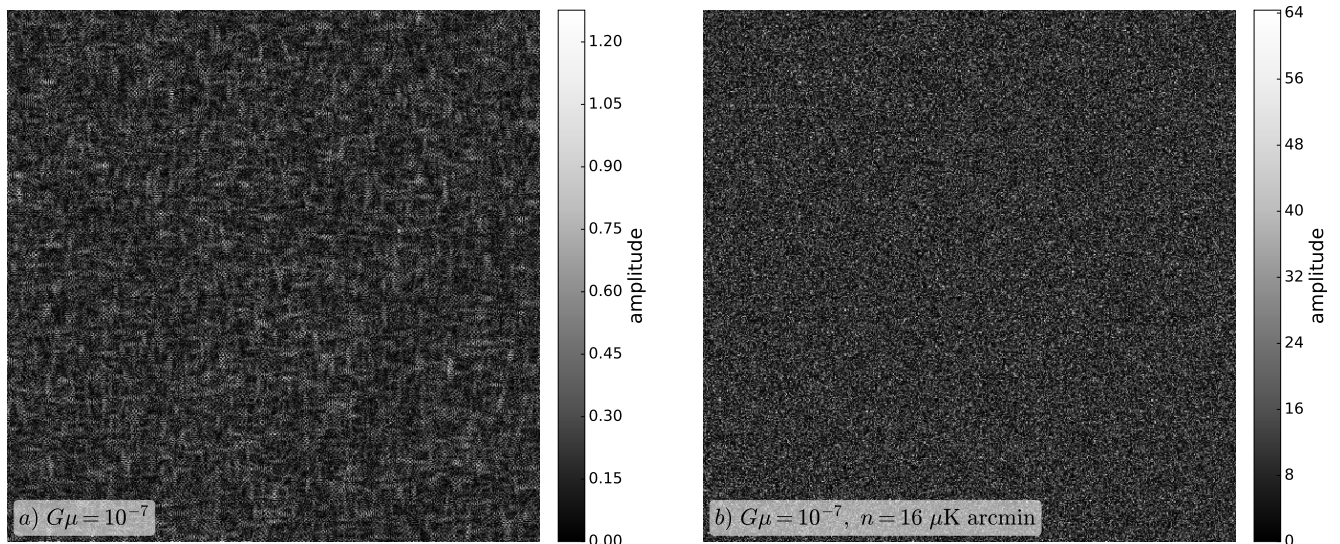


FIG. 6: Reconstruction of the maps from finest scale curvelet images. The left panel corresponds to a CMB anisotropy map with both Gaussian fluctuations and cosmic strings with $G\mu = 10^{-7}$, but without instrumental noise. Here the string signal still are visible by eye. On the right panel, instrumental noise at the level of the SPT-SZ experiment is included and the string signal is no longer visible by eye.

white noise. We find that, at the current noise levels, the Planck maps yield tighter constraints than the SPT-SZ maps, comparable constraints as the SPTpol maps, but that the third generation SPT experiment will be able to provide more stringent constraints than Planck because of the better angular resolution and the reduced noise levels.

V. CONCLUSIONS AND DISCUSSION

In this paper we have explored the potential of extracting signals of cosmic strings from CMB temperature maps using wavelets and curvelets. We have con-

	$G\mu$	k	p_k
Gaussian map		0.055	0.068
CS map	(all)	107.267	< 0.001
combined maps	1×10^{-7}	2.199	< 0.001
	5×10^{-8}	0.204	< 0.001
	4×10^{-8}	0.110	0.001
	3×10^{-8}	0.066	0.036
	2×10^{-8}	0.051	0.105
	1×10^{-8}	0.051	0.101

TABLE II: Excess kurtosis k from the first angle curvelet decomposition and p-value p_k from the kurtosis test for different values of the string tension $G\mu$. (without white noise)

structed temperature maps of the size and angular resolution corresponding to various ongoing CMB experiments containing string signals, Gaussian primordial perturbations, and instrumental noise modelled as white noise, and we have used a KS test on maps with and without string signals to find the level of the string tension for which the string signals can be extracted in a statistically significant way.

With white noise included, we find that the curvelet analysis yields stronger constraints than an analysis based on wavelets, which in turn yields stronger constraints than what can be obtained using the Canny edge detection algorithm. We find that string signals can be seen down to a value $G\mu = 1.4 \times 10^{-7}$ in maps with the specification of the upcoming SPT-3G experiment. This is significantly stronger than corresponding bounds from Planck maps. The improvement is due to the better angular resolution.

Bounds similar to the one we have obtained also result from CMB angular power spectrum analyses [1, 14]. In these analyses, the effect of string-induced fluctuations on the pattern of acoustic oscillations in the CMB is studied. There are other effects which can mimic the effect of cosmic strings on the angular power spectrum (see e.g. [43]). An advantage of our method is that we are looking for signals distinctive to strings. In fact, we have seen that without instrumental noise the strings would be directly visible by eye in wavelet and curvelet images down to a value of $G\mu = 5 \times 10^{-8}$.

Applied to maps with Planck specification, our limits are comparable to what is obtained in [1]. The analyses, however, have complementary strengths and weaknesses.

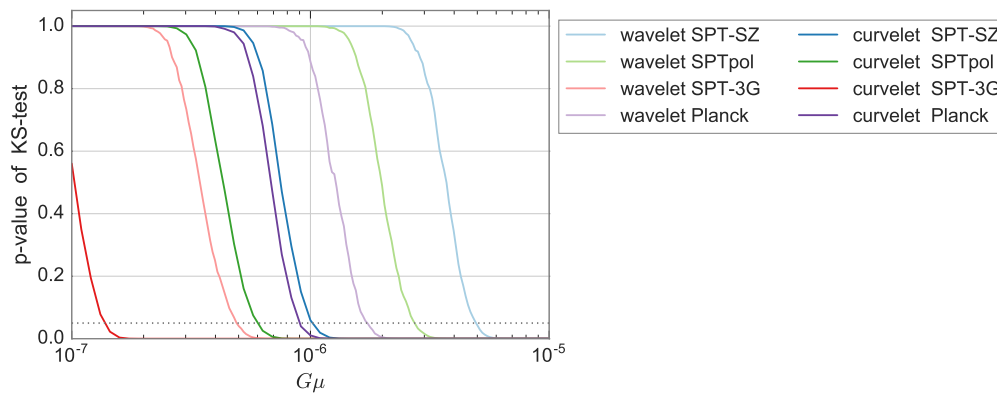


FIG. 7: Comparison of the limits on the cosmic string tension which can be obtained using wavelet and curvelet analyses of SPT and Planck maps. The horizontal axis is the string tension, the vertical axis gives the p-value from a KS test. The dashed horizontal line gives the p-value below which a detection of the string signal is significant. The wavelet analysis made use of the finest scale diagonal details image, the curvelet analysis made use of the first two levels and all angles.

experiment	frequency [GHz]	survey area [deg ²]	resolution [arcmin]	sensitivity [μK arcmin]	$G\mu$ at 95%	
					wavelets	curvelets
SPT-SZ	150	2500	1	16	5×10^{-6}	1×10^{-6}
SPTpol	150	500	1	6	3×10^{-6}	6×10^{-7}
SPT-3G	150	2500	1	1.6	5×10^{-7}	1.4×10^{-7}
Planck	143	32029	7.3	33	1.8×10^{-6}	9×10^{-7}

TABLE III: Parameters of various experiments from [31, 42] used for map generation, and the corresponding $G\mu$ limits (at 95% confidence).

Our analysis focuses on idealized string signals, and we are able to freely vary parameters such as the number N of strings per Hubble volume, and the mean string velocity, parameters which depend on the type of cosmic string evolution simulation being used and on which there is no agreement, while the analysis of [1] uses maps which result from a specific cosmic string simulation. On the other hand, the analysis of [1] is based on less idealized maps which contain the effects not only of the long string segments, but also of string loops and of small-scale structure on the long strings. An obvious advantage of our method is that it is more easily applicable to a range of different experimental designs.

We have only explored one type of mother function for wavelets. There is a lot of room for exploring possible improvement of the detection algorithm by optimizing the mother functions chosen.

On the side of cosmic strings, we have neglected the small-scale structure (see e.g. [44] for some recent studies of small-scale structure on strings) which is expected to build up on the long strings. We have modelled the effects of the small scale structure by taking a narrow band around the temperature discontinuity across the string and replacing δT by 0 in this band. If the width of the

band is taken to be $xy\%$ of the length of the string segment, then we find that the limit on $G\mu$ to which strings can be detected deteriorates by a factor of 2.

A potential followup project would be to apply our wavelet and curvelet algorithms to CMB temperature anisotropy maps constructed from numerical cosmic string evolution simulations (see [33, 34] for a partial list of papers discussing such simulations).

The results of this work encourage us to consider application of wavelet and curvelet statistics to other observational windows, e.g. CMB polarization maps, or three-dimensional 21cm redshift surveys.

Acknowledgement

One of us (RB) wishes to thank the Institute for Theoretical Studies of the ETH Zürich for kind hospitality. RB acknowledges financial support from Dr. Max Rössler, the “Walter Haefner Foundation” and the ETH Zurich Foundation, and from a Simons Foundation fellowship. The research is also supported in part by funds from NSERC and the Canada Research Chair program.

-
- [1] P. A. R. Ade *et al.* [Planck Collaboration], “Planck 2013 results. XXV. Searches for cosmic strings and other topological defects”, *Astron. Astrophys.* **571**, A25 (2014) [arXiv:1303.5085 [astro-ph.CO]].
- [2] A. Vilenkin and E.P.S. Shellard, *Cosmic Strings and other Topological Defects* (Cambridge Univ. Press, Cambridge, 1994).
- [3] M. B. Hindmarsh and T. W. B. Kibble, “Cosmic strings”, *Rept. Prog. Phys.* **58**, 477 (1995) [arXiv:hep-ph/9411342].
- [4] R. H. Brandenberger, “Topological defects and structure formation”, *Int. J. Mod. Phys. A* **9**, 2117 (1994) [arXiv:astro-ph/9310041].
- [5] T. W. B. Kibble, “Phase Transitions In The Early Universe”, *Acta Phys. Polon. B* **13**, 723 (1982);
T. W. B. Kibble, “Some Implications Of A Cosmological Phase Transition”, *Phys. Rept.* **67**, 183 (1980).
- [6] R. H. Brandenberger, “Probing Particle Physics from Top Down with Cosmic Strings”, *Universe* **1**, no. 4, 6 (2013) [arXiv:1401.4619 [astro-ph.CO]].
- [7] A. Vilenkin, “Gravitational Field of Vacuum Domain Walls and Strings”, *Phys. Rev. D* **23**, 852 (1981).
- [8] J. C. R. Magueijo, “Inborn metric of cosmic strings”, *Phys. Rev. D* **46**, 1368 (1992). doi:10.1103/PhysRevD.46.1368
- [9] N. Kaiser and A. Stebbins, “Microwave Anisotropy Due To Cosmic Strings”, *Nature* **310**, 391 (1984).
- [10] Y. B. Zeldovich, “Cosmological fluctuations produced near a singularity”, *Mon. Not. Roy. Astron. Soc.* **192**, 663 (1980).
- [11] A. Vilenkin, “Cosmological Density Fluctuations Produced by Vacuum Strings”, *Phys. Rev. Lett.* **46**, 1169 (1981) Erratum: [*Phys. Rev. Lett.* **46**, 1496 (1981)]. doi:10.1103/PhysRevLett.46.1169, 10.1103/PhysRevLett.46.1496
- [12] N. Turok and R. H. Brandenberger, “Cosmic Strings And The Formation Of Galaxies And Clusters Of Galaxies”, *Phys. Rev. D* **33**, 2175 (1986);
H. Sato, “Galaxy Formation by Cosmic Strings”, *Prog. Theor. Phys.* **75**, 1342 (1986);
A. Stebbins, “Cosmic Strings and Cold Matter”, *Ap. J. (Lett.)* **303**, L21 (1986).
- [13] J. Magueijo, A. Albrecht, D. Coulson and P. Ferreira, “Doppler peaks from active perturbations”, *Phys. Rev. Lett.* **76**, 2617 (1996) [arXiv:astro-ph/9511042];
U. L. Pen, U. Seljak and N. Turok, “Power spectra in global defect theories of cosmic structure formation”, *Phys. Rev. Lett.* **79**, 1611 (1997) [arXiv:astro-ph/9704165];
L. Perivolaropoulos, “Spectral Analysis Of Microwave Background Perturbations Induced By Cosmic Strings”, *Astrophys. J.* **451**, 429 (1995) [arXiv:astro-ph/9402024].
- [14] T. Charnock, A. Avgoustidis, E. J. Copeland and A. Moss, “CMB Constraints on Cosmic Strings and Superstrings”, arXiv:1603.01275 [astro-ph.CO];
C. Dvorkin, M. Wyman and W. Hu, “Cosmic String constraints from WMAP and the South Pole Telescope”, *Phys. Rev. D* **84**, 123519 (2011) [arXiv:1109.4947 [astro-ph.CO]].
- [15] L. Pogosian, S. H. H. Tye, I. Wasserman and M. Wyman, “Observational constraints on cosmic string production during brane inflation”, *Phys. Rev. D* **68**, 023506 (2003) [Erratum-ibid. *D* **73**, 089904 (2006)] [arXiv:hep-th/0304188];
M. Wyman, L. Pogosian and I. Wasserman, “Bounds on cosmic strings from WMAP and SDSS”, *Phys. Rev. D* **72**, 023513 (2005) [Erratum-ibid. *D* **73**, 089905 (2006)] [arXiv:astro-ph/0503364];
A. A. Fraisse, “Limits on Defects Formation and Hybrid Inflationary Models with Three-Year WMAP Observations”, *JCAP* **0703**, 008 (2007) [arXiv:astro-ph/0603589];
U. Seljak, A. Slosar and P. McDonald, “Cosmological parameters from combining the Lyman-alpha forest with CMB, galaxy clustering and SN constraints”, *JCAP* **0610**, 014 (2006) [arXiv:astro-ph/0604335];
R. A. Battye, B. Garbrecht and A. Moss, “Constraints on supersymmetric models of hybrid inflation”, *JCAP* **0609**, 007 (2006) [arXiv:astro-ph/0607339];
R. A. Battye, B. Garbrecht, A. Moss and H. Stoica, “Constraints on Brane Inflation and Cosmic Strings”, *JCAP* **0801**, 020 (2008) [arXiv:0710.1541 [astro-ph]];
N. Bevis, M. Hindmarsh, M. Kunz and J. Urrestilla, “CMB power spectrum contribution from cosmic strings using field-evolution simulations of the Abelian Higgs model”, *Phys. Rev. D* **75**, 065015 (2007) [arXiv:astro-ph/0605018];
N. Bevis, M. Hindmarsh, M. Kunz and J. Urrestilla, “Fitting CMB data with cosmic strings and inflation”, *Phys. Rev. Lett.* **100**, 021301 (2008) [astro-ph/0702223 [ASTRO-PH]];
R. Battye and A. Moss, “Updated constraints on the cosmic string tension”, *Phys. Rev. D* **82**, 023521 (2010) [arXiv:1005.0479 [astro-ph.CO]].
- [16] R. H. Brandenberger, “Searching for Cosmic Strings in New Observational Windows”, *Nucl. Phys. Proc. Suppl.* **246-247**, 45 (2014) doi:10.1016/j.nuclphysbps.2013.10.064 [arXiv:1301.2856 [astro-ph.CO]].
- [17] J. Silk and A. Vilenkin, “Cosmic Strings And Galaxy Formation”, *Phys. Rev. Lett.* **53**, 1700 (1984);
M. J. Rees, “Baryon concentrations in string wakes at $z \gtrsim 200$: implications for galaxy formation and large-scale structure”, *Mon. Not. Roy. Astron. Soc.* **222**, 27 (1986);
T. Vachaspati, “Cosmic Strings and the Large-Scale Structure of the Universe”, *Phys. Rev. Lett.* **57**, 1655 (1986);
A. Stebbins, S. Veeraraghavan, R. H. Brandenberger, J. Silk and N. Turok, “Cosmic String Wakes”, *Astrophys. J.* **322**, 1 (1987).
- [18] R. J. Danos, R. H. Brandenberger and G. Holder, “A Signature of Cosmic Strings Wakes in the CMB Polarization”, *Phys. Rev. D* **82**, 023513 (2010) [arXiv:1003.0905 [astro-ph.CO]].
- [19] R. H. Brandenberger, R. J. Danos, O. F. Hernandez and G. P. Holder, “The 21 cm Signature of Cosmic String Wakes”, *JCAP* **1012**, 028 (2010) [arXiv:1006.2514 [astro-ph.CO]].
- [20] R. H. Brandenberger, O. F. Hernández and D. C. N. da Cunha, “Disruption of Cosmic String Wakes by Gaussian Fluctuations”, arXiv:1508.02317 [astro-ph.CO].

- [21] R. Brandenberger, N. Park and G. Salton, “Angular Power Spectrum of B-mode Polarization from Cosmic String Wakes”, arXiv:1308.5693 [astro-ph.CO].
- [22] Ruch, David K.; Van Fleet, Patrick J. (2009). Wavelet Theory: An Elementary Approach with Applications. John Wiley & Sons.;
A. Graps. An introduction to wavelets. Computational Science Engineering, IEEE, 2(2), 50 - 61, Summer 1995.
- [23] E.J. Candès, D.L. Donoho, “Curvelets: a surprisingly effective nonadaptive representation of objects with edges”, A. Cohen, C. Rabut, L.L. Schumaker (Eds.), “Curve and Surface Fitting: Saint-Malo 1999”, Vanderbilt University Press, Nashville (2000)
- [24] E. Jeong and G. F. Smoot, “Search for cosmic strings in CMB anisotropies”, *Astrophys. J.* **624**, 21 (2005) doi:10.1086/428921 [astro-ph/0406432].
- [25] A. S. Lo and E. L. Wright, “Signatures of cosmic strings in the cosmic microwave background”, astro-ph/0503120.
- [26] J. Canny, “A computational approach to edge detection”, *IEEE Trans. Pattern Analysis and Machine Intelligence* **8**, 679 (1986).
- [27] R. J. Danos and R. H. Brandenberger, “Canny Algorithm, Cosmic Strings and the Cosmic Microwave Background”, *Int. J. Mod. Phys. D* **19**, 183 (2010) [arXiv:0811.2004 [astro-ph]];
S. Amsel, J. Berger and R. H. Brandenberger, “Detecting Cosmic Strings in the CMB with the Canny Algorithm”, *JCAP* **0804**, 015 (2008) [arXiv:0709.0982 [astro-ph]];
A. Stewart and R. Brandenberger, “Edge Detection, Cosmic Strings and the South Pole Telescope”, *JCAP* **0902**, 009 (2009) [arXiv:0809.0865 [astro-ph]].
- [28] J. E. Ruhl *et al.* [The SPT Collaboration], “The South Pole Telescope”, *Proc. SPIE Int. Soc. Opt. Eng.* **5498**, 11 (2004) [arXiv:astro-ph/0411122].
- [29] A. Kosowsky [the ACT Collaboration], “The Atacama Cosmology Telescope Project: A Progress Report”, *New Astron. Rev.* **50**, 969 (2006) [arXiv:astro-ph/0608549].
- [30] P. A. R. Ade *et al.* [Planck Collaboration], “Planck 2013 results. I. Overview of products and scientific results”, *Astron. Astrophys.* **571**, A1 (2014) doi:10.1051/0004-6361/201321529 [arXiv:1303.5062 [astro-ph.CO]].
- [31] B. A. Benson *et al.* [SPT-3G Collaboration], “SPT-3G: A Next-Generation Cosmic Microwave Background Polarization Experiment on the South Pole Telescope”, *Proc. SPIE Int. Soc. Opt. Eng.* **9153**, 91531P (2014) doi:10.1117/12.2057305 [arXiv:1407.2973 [astro-ph.IM]].
- [32] J. L. Starck, N. Aghanim and O. Forni, “Detection and discrimination of cosmological non-gaussian signatures by multi-scale methods”, *Astron. Astrophys.* **416**, 9 (2004) doi:10.1051/0004-6361:20040067 [astro-ph/0311577].
- [33] C. Ringeval and F. R. Bouchet, “All Sky CMB Map from Cosmic Strings Integrated Sachs-Wolfe Effect”, *Phys. Rev. D* **86**, 023513 (2012) doi:10.1103/PhysRevD.86.023513 [arXiv:1204.5041 [astro-ph.CO]].
- [34] A. Albrecht and N. Turok, “Evolution Of Cosmic Strings”, *Phys. Rev. Lett.* **54**, 1868 (1985);
D. P. Bennett and F. R. Bouchet, “Evidence For A Scaling Solution In Cosmic String Evolution”, *Phys. Rev. Lett.* **60**, 257 (1988);
B. Allen and E. P. S. Shellard, “Cosmic String Evolution: A Numerical Simulation”, *Phys. Rev. Lett.* **64**, 119 (1990);
C. Ringeval, M. Sakellariadou and F. Bouchet, “Cosmological evolution of cosmic string loops”, *JCAP* **0702**, 023 (2007) [arXiv:astro-ph/0511646];
V. Vanchurin, K. D. Olum and A. Vilenkin, “Scaling of cosmic string loops”, *Phys. Rev. D* **74**, 063527 (2006) [arXiv:gr-qc/0511159];
L. Lorenz, C. Ringeval and M. Sakellariadou, “Cosmic string loop distribution on all length scales and at any redshift”, *JCAP* **1010**, 003 (2010) [arXiv:1006.0931 [astro-ph.CO]];
J. J. Blanco-Pillado, K. D. Olum and B. Shlaer, “Large parallel cosmic string simulations: New results on loop production”, *Phys. Rev. D* **83**, 083514 (2011) [arXiv:1101.5173 [astro-ph.CO]];
J. J. Blanco-Pillado, K. D. Olum and B. Shlaer, “The number of cosmic string loops”, *Phys. Rev. D* **89**, no. 2, 023512 (2014) [arXiv:1309.6637 [astro-ph.CO]].
- [35] A. Lewis and S. Bridle, “Cosmological parameters from CMB and other data: A Monte Carlo approach”, *Phys. Rev. D* **66**, 103511 (2002) doi:10.1103/PhysRevD.66.103511 [astro-ph/0205436].
- [36] L. Perivolaropoulos, “COBE versus cosmic strings: An Analytical model”, *Phys. Lett. B* **298**, 305 (1993) [arXiv:hep-ph/9208247];
L. Perivolaropoulos, “Statistics of microwave fluctuations induced by topological defects”, *Phys. Rev. D* **48**, 1530 (1993) [arXiv:hep-ph/9212228].
- [37] J. J. Blanco-Pillado, K. D. Olum and B. Shlaer, “Large parallel cosmic string simulations: New results on loop production”, *Phys. Rev. D* **83**, 083514 (2011) doi:10.1103/PhysRevD.83.083514 [arXiv:1101.5173 [astro-ph.CO]].
- [38] I. Daubechies, “The Wavelet transform, time frequency localization and signal analysis”, *IEEE Trans. Info. Theor.* **36**, 961 (1990). doi:10.1109/18.57199
- [39] Emmanuel Candes, Laurent Demanet, David Donoho, and Lexing Ying. “Fast discrete curvelet transforms. Multiscale Modeling & Simulation”, 5(3), 861 - 899, 2006.
- [40] K. T. Story *et al.*, “A Measurement of the Cosmic Microwave Background Damping Tail from the 2500-Square-Degree SPT-SZ Survey”, *Astrophys. J.* **779**, 1 (2013) doi:10.1088/0004-637X/779/1/86 [arXiv:1210.7231 [astro-ph.CO]].
- [41] J. E. Austermann *et al.*, “SPTpol: an instrument for CMB polarization measurements with the South Pole Telescope”, *Proc. SPIE Int. Soc. Opt. Eng.* **8452**, 84521E (2012) doi:10.1117/12.927286 [arXiv:1210.4970 [astro-ph.IM]].
- [42] Planck Collaboration, “Planck 2015 results. VIII. High Frequency Instrument data processing: Calibration and maps”, *A&A*, Forthcoming article doi:10.1051/0004-6361/201525820 [arXiv:1502.01587 [astro-ph.CO]].
- [43] N. Turok, “A Causal source which mimics inflation”, *Phys. Rev. Lett.* **77**, 4138 (1996) doi:10.1103/PhysRevLett.77.4138 [astro-ph/9607109].
- [44] J. Polchinski and J. V. Rocha, “Analytic study of small scale structure on cosmic strings”, *Phys. Rev. D* **74**, 083504 (2006) doi:10.1103/PhysRevD.74.083504 [hep-ph/0606205];
M. Hindmarsh, S. Stuckey and N. Bevis, “Abelian Higgs Cosmic Strings: Small Scale Structure and Loops”, *Phys. Rev. D* **79**, 123504 (2009) doi:10.1103/PhysRevD.79.123504 [arXiv:0812.1929 [hep-th]];

E. J. Copeland and T. W. B. Kibble, “Kinks and small-scale structure on cosmic strings”, *Phys. Rev. D* **80**, 123523 (2009) doi:10.1103/PhysRevD.80.123523

[arXiv:0909.1960 [astro-ph.CO]].